Numerical Simulation of Viscoelastic Free Surface Flows Using the Second Order Fluid Constitutive Equation

José Laércio Doricio
ICMC-USP
josedoricio@yahoo.com.br

Murilo Francisco Tomé
ICMC-USP
murilo@icmc.usp.br

Antônio Castelo Filho
ICMC-USP
castelo@icmc.usp.br

José Alberto Cuminato
ICMC-USP
jacumina@icmc.usp.br

Valdemir G. Ferreira
ICMC-USP
pvgf@icmc.usp.br

Abstract. *This work deals with the numerical simulation of unsteady viscoelastic free surface flows of a Second Order fluid. The governing equations are solved using a finite difference technique based on a Marker-and-Cell methodology. A staggered grid is employed and marker particles are used to represent the fluid providing fluid flow visualization and the location of the fluid free surface. Full details for the approximation of the boundary conditions on the free surface are given. The convective terms are approximated by a high order upwind method. Numerical results demonstrating the capabilities of this technique in solving viscoelastic free surface flows of a Second Order fluid are presented for a number of problems involving transient free surface flows. In particular, we present numerical simulations of the extrudate swell for various Deborah numbers. In addition, validation and convergence results are given.*

Keywords: *Second order fluid, Free surface flow, Finite difference, Marker-and-cell.*

1. Introduction

Polymer processing appears in many industrial applications such as extrusion and fiber-spinning, container filling, wire coating, among others. Therefore, there is a strong interest in developing numerical techniques for investigating polymer fluid flows. For Newtonian flows there are many techniques capable of solving complex free surface flows (see the books by Shyy (1997) and Griebel et al. (1999)). A review of these techniques is presented by McKee et al. (2003). Nowadays there is a trendy for developing numerical techniques for solving non-Newtonian fluid flows. The Maxwell, Oldroyd-B and PTT models have been studied by many researchers and a variety of techniques for simulating viscoelastic flows governed by these models have been presented, eg. Yoo and Na (1991), Marchal and Crochet (1987), Carew et al. (1993), Brasseur et al. (1998), Huang et al. (1996), Phillips and Williams (1999), Xue et al. (1998), to cite a few. The problems investigated have been the contraction 4:1 problem in two (eg. Phillips and Williams (1999), Yoo and Na (1991), Sato and Richardson (1994)) and three dimensions (eg. Mompean and Deville (1997), Xue et al. (1998)) and the extrudate swell problem (see. Ryan and Dutta (1981), Crochet and Keunings (1982), Brasseur et al. (1998), Tomé et al. (2002)). Viscoelastic flows governed by the CEF (Criminale-Ericksen-Filbey) constitutive equation have been trackled by a few authors. Among the researchers who investigated flows of the Second Order fluid, we can mention the work of Gast and Ellingson (1999). They considered the Second Order fluid model and by using the Fidap code presented numerical results for the extrudate swell of fluids having small viscoelasticity.

In this work we present a numerical technique for solving the Second Order fluid flow model for free surface flows. We formulate a MAC (Marker-and-Cell) (Harlow and Welch (1965)) type numerical algorithm for solving the governing equations and develop a finite difference method for solving the basic equations. The method described herein is validate by using exact solutions for two-dimensional channel flow and numerical results of the time-dependent extrudate swell are presented.

2. Basic Equations

The equations governing two-dimensional Cartesian flows of a Second Order fluid can be written, in nondimensional form, as (see Doricio (2003))

$$\frac{\partial u}{\partial x}+\frac{\partial v}{\partial y}=0 \tag{1}$$

$$\frac{\partial u}{\partial t}+\frac{\partial u^2}{\partial x}+\frac{\partial uv}{\partial y}=-\frac{\partial p}{\partial x}+\frac{1}{Re}\left[\frac{\partial^2 u}{\partial x^2}+\frac{\partial^2 u}{\partial y^2}+\frac{\partial \Phi^{xx}}{\partial x}+\frac{\partial \Phi^{xy}}{\partial y}\right]+\frac{1}{Fr^2}g_x\ , \tag{2}$$

$$\frac{\partial v}{\partial t}+\frac{\partial uv}{\partial x}+\frac{\partial v^2}{\partial y}=-\frac{\partial p}{\partial y}+\frac{1}{Re}\left[\frac{\partial^2 v}{\partial x^2}+\frac{\partial^2 v}{\partial y^2}+\frac{\partial \Phi^{xy}}{\partial x}+\frac{\partial \Phi^{yy}}{\partial y}\right]+\frac{1}{Fr^2}g_y\ , \tag{3}$$

$$\tau^{xx}=\frac{1}{Re}\left(\mathrm{D}^{xx}+\Phi^{xx}\right)\ ,\quad \tau^{xy}=\frac{1}{Re}\left(\mathrm{D}^{xy}+\Phi^{xy}\right)\ ,\quad \tau^{yy}=\frac{1}{Re}\left(\mathrm{D}^{yy}+\Phi^{yy}\right)\ , \tag{4}$$

where $\mathrm{D}^{xx}, \mathrm{D}^{xy}$ and D^{yy} are given by

$$\mathrm{D}^{xx}=\frac{\partial u}{\partial x}\ ,\quad \mathrm{D}^{xy}=\frac{\partial u}{\partial y}+\frac{\partial v}{\partial x}\ ,\quad \mathrm{D}^{yy}=\frac{\partial v}{\partial y} \tag{5}$$

and the rheological functions are given by

$$\Phi^{xx} = \kappa\left[4\left(\frac{\partial u}{\partial x}\right)^2+\left(\frac{\partial u}{\partial y}+\frac{\partial v}{\partial x}\right)^2\right]-De\left[-\frac{D(\mathrm{D}^{xx})}{Dt}+4\left(\frac{\partial u}{\partial x}\right)^2+2\frac{\partial u}{\partial y}\left(\frac{\partial u}{\partial y}+\frac{\partial v}{\partial x}\right)\right]\ , \tag{6}$$

$$\Phi^{xy} = -2De\left[-\frac{D(\mathrm{D}^{xy})}{Dt}+\frac{\partial u}{\partial x}\frac{\partial v}{\partial x}+\frac{\partial u}{\partial y}\frac{\partial v}{\partial y}\right]\ , \tag{7}$$

$$\Phi^{yy} = \kappa\left[4\left(\frac{\partial v}{\partial y}\right)^2+\left(\frac{\partial u}{\partial y}+\frac{\partial v}{\partial x}\right)^2\right]-De\left[-\frac{D(\mathrm{D}^{yy})}{Dt}+4\left(\frac{\partial v}{\partial y}\right)^2+2\frac{\partial v}{\partial x}\left(\frac{\partial u}{\partial y}+\frac{\partial v}{\partial x}\right)\right], \tag{8}$$

where $Re=\frac{\rho UL}{\eta_0}, Fr=\frac{U}{\sqrt{Lg}}, De=\frac{\lambda_2 U}{L}$ are the Reynolds number, Froude number and the Deborah number, respectively. The nondimensional number κ is defined by $\kappa=\frac{\lambda_4 U}{L}$. The symbol $\frac{\mathrm{D}}{Dt}$ refers to the material derivative. In steady shear flows, the material parameters λ_2 and λ_4 are related to the coefficients of the first and second normal stress differences

$$\psi_1=2\eta_0\lambda_2=\frac{N_1}{(\mathrm{D}^{xy})^2}=\frac{\tau_{11}-\tau_{22}}{(\mathrm{D}^{xy})^2}\ ,\quad \psi_2=2\eta_0\lambda_4=\frac{N_2}{(\mathrm{D}^{xy})^2}=\frac{\tau_{22}-\tau_{33}}{(\mathrm{D}^{xy})^2}\ .$$

The material parameter λ_4 is found, experimentally, to be much less than λ_2 (usually $\lambda_4\approx 0.1\lambda_2$) and is related to the second normal stress difference. Therefore, in this work we shall neglect any contributions from the nondimensional number $\kappa=\frac{\lambda_4 U}{L}$. This means that the problems to be solved have no second normal stress difference, i.e., $\lambda_4=0$).

2.1 Computation of the rheological function Φ^{xy} on rigid boundaries and inflows and outflows

When solving Eq. (2) and Eq. (3) the values of Φ^{xy} on rigid boundaries, inflows and outflows are required. These can be obtained from Eq. (7) as follows:

- Rigid boundaries: if we consider rigid boundaries which are parallel to the x-axis we have:

  $$\frac{\partial u}{\partial x}=0,\qquad \frac{\partial v}{\partial x}=0,\qquad \frac{\partial v}{\partial y}=0\quad \text{from mass conservation}$$

  Introducing these derivatives into Eq. (7) one finds that on rigid boundaries which are parallel to the x-axis we have $\Phi^{xy}=0$. On the other hand, if the rigid boundary is parallel to the y-axis then it can be verified that in this case we obtain $\Phi^{xy}=0$.

- Inflows: if the velocity at the inflow is prescribed by $u=U_{inf}$ and $v=V_{inf}$ than the values of Φ^{xy} on inflows are the same as those for Φ^{xy} on rigid boundaries. However, we shall have inflows defined by $u=u(y), v=0$, if the inflow is vertical or $u=0, v=v(x)$, in the case of a horizontal inflow; the velocity $u(y)$ (or $v(x)$) is a parabolic function of y. In this case, it can be shown that the value of Φ^{xy} on inflows is zero.

- Outflows: at the fluid exit we have the condition $\frac{\partial u_T}{\partial n}=0$ where u_T is the tangential velocity to the outflow and n is the normal direction. Thus, if the outflow is situated parallel to the y-axis we have $\frac{\partial v}{\partial x}=0$; in this case it can be found that $\Phi^{xy}=0$.

2.2 Numerical method

To solve Eq. (1) to Eq. (8) we employ a methodology based on the GENSMAC algorithm (see Tomé et al. (1996)). We suppose that the velocity field $\mathbf{u}(\mathbf{x}, t_n)$ is known and boundary conditions for velocity and pressure are given. The velocity and pressure fields at time $t = t_n + \delta t$ are calculated as follows:

First, by using $\mathbf{u}(\mathbf{x}, t_n)$ we compute the components of the rate-of-deformation tensor, D^{xx}, D^{xy} and D^{yy} and then calculate the rheological functions $\Phi^{xx}, \Phi^{xy}, \Phi^{yy}$ everywhere in the mesh. The finite difference equations for calculating $\Phi^{xx}, \Phi^{xy}, \Phi^{yy}$ are given in Section 4.1. Now, let $\widetilde{p}(\mathbf{x}, t)$ be a pressure field which coincides with the correct pressure condition on the free surface. This pressure field is calculated from Eq. (18). Details on the calculation of $\widetilde{p}(\mathbf{x}, t)$ can be found in Doricio (2003). Inserting $\widetilde{p}(\mathbf{x}, t)$ into Eq. (2) and Eq. (3) we compute a tentative velocity field $\widetilde{\mathbf{u}}(\mathbf{x}, t)$ from

$$\frac{\partial \widetilde{u}}{\partial t} + \frac{\partial u^2}{\partial x} + \frac{\partial uv}{\partial y} = -\frac{\partial \widetilde{p}}{\partial x} + \frac{1}{Re}\left[\frac{\partial^2 u}{\partial x^2} + \frac{\partial^2 u}{\partial y^2} + \frac{\partial \Phi^{xx}}{\partial x} + \frac{\partial \Phi^{xy}}{\partial y}\right] + \frac{1}{Fr^2} g_x \,, \tag{9}$$

$$\frac{\partial \widetilde{v}}{\partial t} + \frac{\partial uv}{\partial x} + \frac{\partial v^2}{\partial y} = -\frac{\partial \widetilde{p}}{\partial y} + \frac{1}{Re}\left[\frac{\partial^2 v}{\partial x^2} + \frac{\partial^2 v}{\partial y^2} + \frac{\partial \Phi^{xy}}{\partial x} + \frac{\partial \Phi^{yy}}{\partial y}\right] + \frac{1}{Fr^2} g_y \,, \tag{10}$$

with $\widetilde{\mathbf{u}}(\mathbf{x}, t_n) = \mathbf{u}(\mathbf{x}, t_n)$ using the appropriate boundary conditions for $\widetilde{\mathbf{u}}(\mathbf{x}, t)$ at $t = t_n$. The Eq. (9) and Eq. (10) are solved by an explicit finite difference method. It can be shown (see Tomé et al. 1996) that $\widetilde{\mathbf{u}}(\mathbf{x}, t)$ possesses the correct vorticity at time t. However, $\widetilde{\mathbf{u}}(\mathbf{x}, t)$ does not conserve mass. Let $\mathbf{u}(\mathbf{x}, t)$ be defined by

$$\mathbf{u}(\mathbf{x}, t) - \widetilde{\mathbf{u}}(\mathbf{x}, t) = -\nabla \psi(\mathbf{x}, t) \tag{11}$$

where $\psi(\mathbf{x}, t)$ is a function having the property

$$\nabla^2 \psi(\mathbf{x}, t) = \nabla \cdot \widetilde{\mathbf{u}}(\mathbf{x}, t) \,. \tag{12}$$

Thus, $\mathbf{u}(\mathbf{x}, t)$ conserves mass and possesses the correct vorticity at time t. An equation for pressure is obtained as follows. By subtracting Eq. (2) from Eq. (9) and Eq. (3) from Eq. (10) we can write

$$\frac{\partial(\mathbf{u} - \widetilde{\mathbf{u}})}{\partial t} = -\nabla(p(\mathbf{x}, t) - \widetilde{p}(\mathbf{x}, t)) \,. \tag{13}$$

Now, introducing Eq. (11) into Eq. (13) it yields

$$-\frac{\partial}{\partial t}\nabla \psi(\mathbf{x}, t) = -\nabla(p(\mathbf{x}, t) - \widetilde{p}(\mathbf{x}, t)) \tag{14}$$

and interchanging the operators in Eq. (14) we obtain

$$p(\mathbf{x}, t) = \widetilde{p}(\mathbf{x}, t) + \frac{\partial \psi(\mathbf{x}, t)}{\partial t} \tag{15}$$

which is evaluated as

$$p(\mathbf{x}, t) = \widetilde{p}(\mathbf{x}, t) + \frac{\psi(\mathbf{x}, t)}{\delta t} \,. \tag{16}$$

Therefore, for simulating flows governed by the Second Order constitutive equation we have to solve Eq. (9), Eq. (10), Eq. (12), Eq. (11) and Eq. (16), respectively.

3. Finite Difference Approximation

For solving Eq. (9) to Eq. (16) we employ the finite difference method as follows.

A staggered grid is used (see Fig. 1a). The pressure and the rheological functions are positioned at the cell centre while the velocity components are staggered by a factor of $\delta x/2$, $\delta y/2$, respectively. As the fluid is moving, a scheme for identifying the fluid region and the free surface is employed. To affect this, the cells within the mesh can be of several types: empty cell (E) if it has no fluid in it, full cell (F) if the cell has fluid and has no face in contact with an empty cell face, surface cell (S) if the cell has fluid and has at least one face in contact with empty cell faces, boundary cell (B) if it define a rigid boundary, inflow cell (I) if it defines an inflow boundary and outflow cell (O) if it defines an outflow boundary. "Figure 1b" illustrates the types of cells which can be present in a calculation time step; the empty cells were left blank for convenience.

The momentum equations, Eq. (9) and Eq. (10), are approximated by finite differences as follows: the time derivative is approximated by the explicit Euler method and the linear spatial terms are discretized by central differences. The convective terms are approximated by a high order upwind method. In this work we have used the VONOS method (see Varonos and Bergeles (1998)). Details of the implementation can be found in Ferreira et al. (2002). The corresponding finite difference approximation of Eq. (9), Eq. (10), Eq. (12), Eq. (11) and Eq. (16) can be found in Doricio (2003).

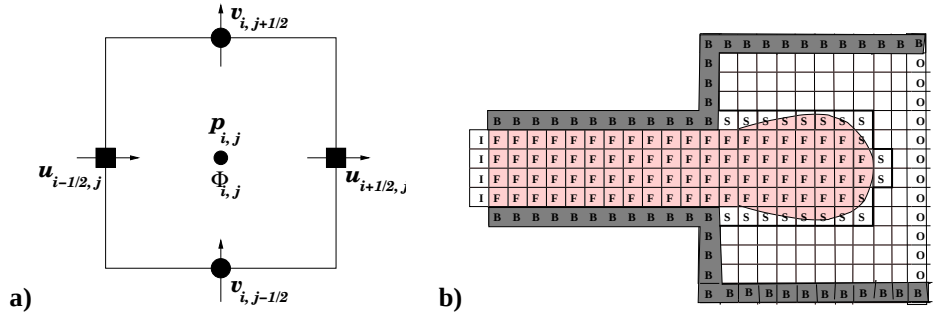

Figure 1. **a)** Cell configuration for a Second Order fluid flow calculation, **b)** Types of cells within the mesh.

3.1 Finite Difference Approximation of the Free Surface Stress Conditions

Let $\mathbf{n} = (n_x, n_y)$ and $\mathbf{m} = (n_y, -n_x)$ denote unit normal and tangential vectors to the free surface, respectively. Then, the stress conditions can be written as (see Doricio (2003))

$$p - \frac{1}{Re}\left[(\mathrm{D}^{xx} + \Phi^{xx})n_x^2 + (\mathrm{D}^{yy} + \Phi^{yy})n_y^2 + 2(\mathrm{D}^{xy} + \Phi^{xy})n_x n_y\right] = 0\,, \tag{17}$$

$$\frac{2}{Re}\left[(\mathrm{D}^{xx} - \mathrm{D}^{yy} + \Phi^{xx} - \Phi^{yy})\,n_x\,n_y + (\mathrm{D}^{xy} + \Phi^{xy})\,(n_x^2 - n_y^2)\right] = 0\,. \tag{18}$$

We point out that the problems we intend to solve have a low Reynolds number and therefore when applying conditions above we shall neglect the convective terms from the material derivative appearing in the computation of the rheological functions $\phi^{xx}, \phi^{xy}, \phi^{yy}$. In order to apply these conditions we follow the ideas adopted by Tomé et al. (1996). We suppose the mesh spacing is sufficient small so that the free surface can be represented, locally, by a linear surface which is either parallel to the one coordinate axis or is a 45^o sloped surface. Details of the finite difference equations involved are given in Doricio (2003).

3.2 Time-step control and particle movement

A time-step procedure for calculating the time-step size for every computational cycle is employed. This procedure was presented by Tomé and McKee (1994) for Newtonian flows and is based on the stability restrictions

$$\begin{aligned} \delta t_1 &< \frac{\delta \mathbf{x}}{\max|\mathbf{u}_{max}|}\,, \quad \delta t_2 < \frac{\delta x^2}{4} Re \quad \text{(here it is assumed that } \delta x = \delta y)\,, \\ \delta t &= FACT * \min(\delta t_1, \delta t_2) \quad \text{where} \quad 0 < FACT < 1\,. \end{aligned} \tag{19}$$

The factor $FACT$ is employed as a conservative measure to allow the fact that the stability analysis has been performed locally and the value of $\max|\mathbf{u}_{max}|$ is not known a priori. Details of the implementation of this time-step procedure is given by Tomé and McKee (1994). Usually, when simulating Newtonian flows the factor FACT takes the value of 0.5. However, for second order fluid flow simulations a more restrictive value is used depending on the value of the Deborah number De. In the results presented in this paper we used a value of 0.1 for the factor $FACT$.

Once the final velocities have been calculated the last step of the numerical method described in Section 3 is to update the marker particle positions. The new markers positions are obtained by solving

$$\frac{d\mathbf{x}_p}{dt} = \mathbf{u}_p \tag{20}$$

by using the explicit improved Euler method. The particle velocity $\mathbf{u}_p$ is found by performing a bilinear interpolation using the nearest four node velocities. Details of the particle movement can be found in Tomé and McKee (1994).

4. Convergence and numerical results

The finite difference equations described in Section 4 have been implemented into the FreeFlow-2D code in order to simulate flows of an Second Order Fluid. In this section we present results to validate the numerical method and the implementation of the governing equations as well as some numerical results which show viscoelastic behaviour.

4.1 Validation of the approach

We validate the numerical method presented in this paper by simulating the flow in a two-dimensional channel. We consider a channel having an entrance with a width of L and a lenght of $15L$. At the channel entrance we prescribe a fully

developed flow defined by

$$u(y) = -4\frac{U}{L}\left(y - \frac{L}{2}\right)^2 + U \; . \tag{21}$$

On the channel walls velocity field satisfies the no-slip condition while at the outflow Neumann conditions are assumed. We start with the channel empty and inject fluid at the inflow until the channel is full and steady state is reached. It can be seen that under steady state conditions the components of the extra stress tensor (see Eq. (4)) reduce to

$$\tau^{xx} = -\frac{2}{Re}\left(\frac{\partial u}{\partial y}\right)^2 \; , \quad \tau^{xy} = \frac{1}{Re}\left(\frac{\partial u}{\partial y}\right) \; , \quad \tau^{yy} = 0 \; . \tag{22}$$

We point out that under steady state conditions Eq. (21) to Eq. (22) are valid throught the channel. To simulate this problem we used the following input data: $L = 1\text{cm}$, $U = 1\text{ms}^{-1}$ and gravity was neglected ($g_x = g_y = 0$). The material properties were $\nu_0 = \frac{\eta_0}{\rho} = 0.01\text{m}^2\text{s}^{-1}$ and $\lambda_2 = 0.0045\text{s}$. The scaling parameters were L, U and ν_0 giving $Re = UL/\nu_0 = 1$ and $De = \lambda_2 U/L = 0.45$. To demonstrate the convergence of the numerical method presented in this paper we ran this problem using three meshes: **Mesh1** - $\delta x = \delta y = 0.125\text{cm}$ (8×120 cells); **Mesh2** - $\delta x = \delta y = 0.0625\text{cm}$ (16×240 cells) and **Mesh3** - $\delta x = \delta y = 0.03125\text{cm}$ (32×480 cells). All the three runs achieved steady state. The time evolution of the contour lines of velocity u obtained on **Mesh3** is shown in Fig. 2. We can see in Fig. 2**b)** that the

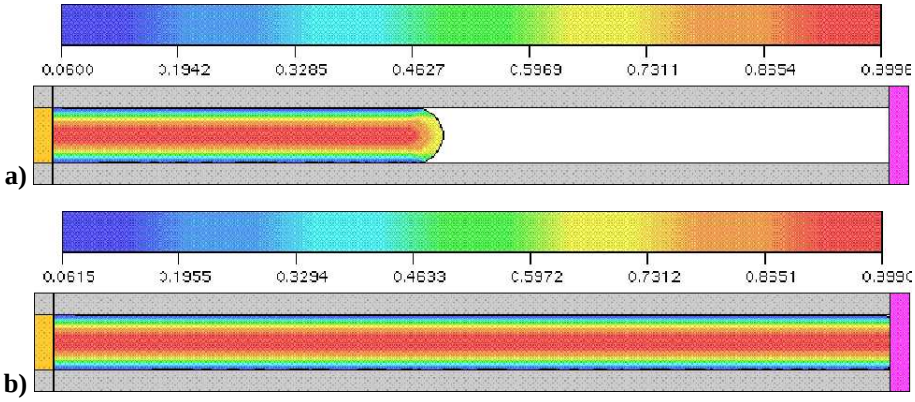

Figure 2. Channel flow simulation: contour lines of velocity u at times $t = 0.1s$ (**a)**) and $t = 0.545s$ (**b)**). Results obtained on **Mesh 3**.

contour lines are all parallel indicating that the steady state was reached. "Figure 3" shows the numerical results obtained for the extra-stress components τ^{xx} and τ^{xy} and the velocity component u at the middle of the channel ($x = 7.5$) using **Mesh1** and Fig. 4 displays the numerical results obtained on **Mesh2**. The numerical results on **Mesh3** are displayed in Fig. 5. As we can see in Fig. 3, Fig. 4 and Fig. 5, the agreement between the numerical results and the exact solution for the velocity field on the three meshes is very good. The numerical results for the extra-stress components τ^{xx} and τ^{xy} near the channel walls using **Mesh1** do not agree very well with the exact solutions. However, as the mesh is refined (see Fig. 4 and Fig. 5) we can see that the values of the u, τ^{xx} and τ^{xy} approach the values of the respective exact solutions everywhere. This shows the convergence of the numerical method presented in this paper.

4.2 Numerical simulation of the extrudate swell of a Second Order fluid

To demonstrate that the numerical method presented in this paper can cope with high elastic fluids governed by the Second Order fluid constitutive equation we present several simulations of the extrudate swell with increasing Deborah numbers. The input data describing the computational domain are displayed in Fig. 6. On the channel walls the velocity field obeys the no-slip condition while on the free surface the stress conditions (see Eq. (17) and Eq. (18) are imposed. At the fluid entrance the velocity is prescribed by a parabolic profile given by Eq. (21) where $U = 1\text{ ms}^{-1}$. The domain size was $15\text{ cm} \times 3\text{ cm}$ and a mesh size of $\delta x = \delta y = 0.0625\text{ cm}$ (208×48 cells within the domain) was employed. Gravity was neglected and the value of the kinematic viscosity was $\nu_0 = 0.01\text{ m}^2\text{s}^{-1}$. The constant λ_2 took the values of 0.002 s, 0.004 s, 0.006 s and 0.008 s. The scaling parameters were U, D and ν_0 and therefore $Re = UD/\nu_0 = 1$ and the Deborah numbers were $De = 0.2, 0.4, 0.6, 0.8$, respectively. The fluid flow configuration of these simulations are displayed in Fig. 7. We can see in Fig. 7 that as we increase the value De the swelling ratios $S_r = D_{max}/D$ increase. Indeed, in these simulations we obtained $S_r = 1.42$ for $De = 0.2$ and $S_r = 1.85$ for $De = 0.8$ which shows that the numerical method presented in this paper can indeed deal with high elastic fluids.

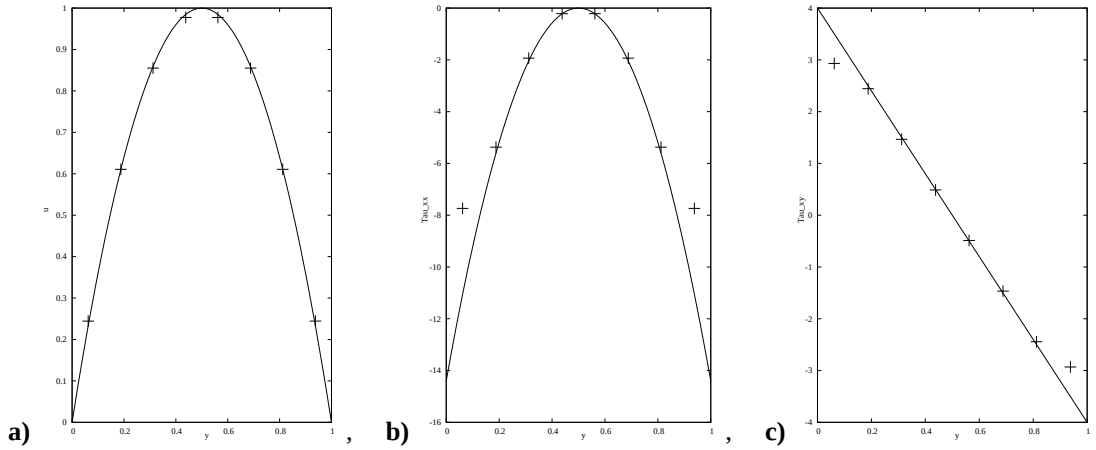

Figure 3. Numerical simulation of channel flow with $Re = 1$ and $De = 0.45$ (symbols) using **Mesh1**. Comparison with analytic solutions (solid lines). **a)** velocity u, **b)** extra-stress component τ^{xx}, **c)** extra-stress component τ_{xy}. Results shown at position $x = 7.5$ cm.

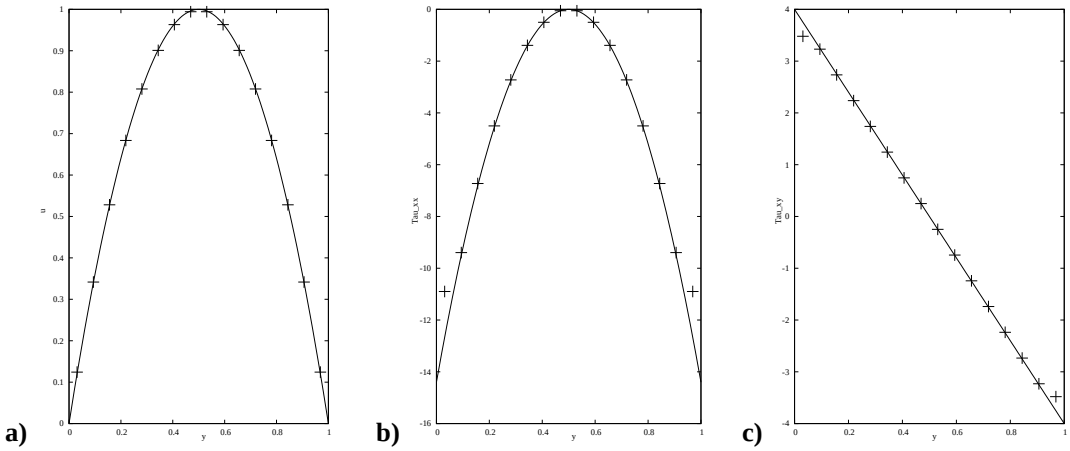

Figure 4. Numerical simulation of the channel flow with $Re = 1$ and $De = 0.45$ (symbols) on **Mesh2**. Comparison with analytic solutions (solid lines). **a)** velocity u, **b)** extra-stress component τ_{xx}, **c)** extra-stress component τ_{xy}. Results shown at position $x = 7.5$ cm.

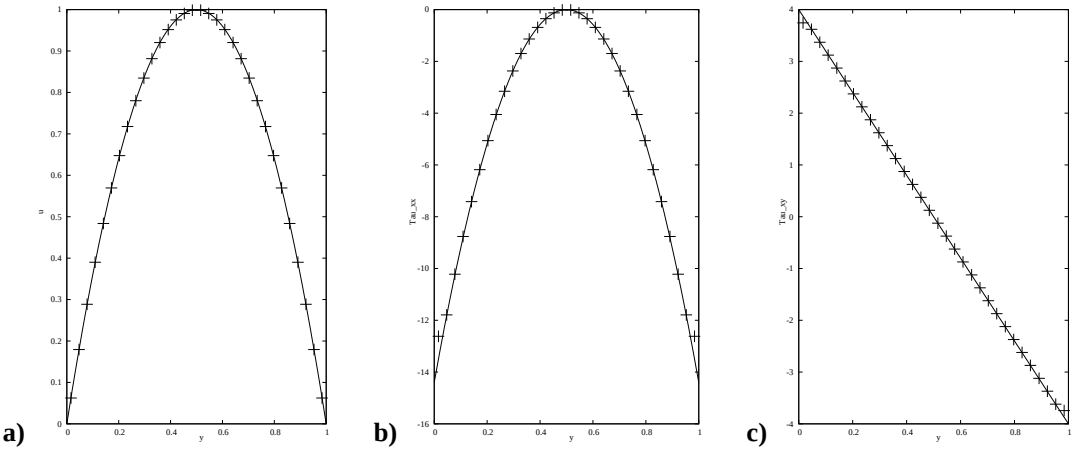

Figure 5. Numerical simulation of the channel flow with $Re = 1$ and $De = 0.45$ (symbols) using **Mesh3**. Comparison with analytic solutions (solid lines). **a)** velocity u, **b)** extra-stress component τ_{xx}, **c)** extra-stress component τ_{xy}. Results shown at position $x = 7.5$ cm.

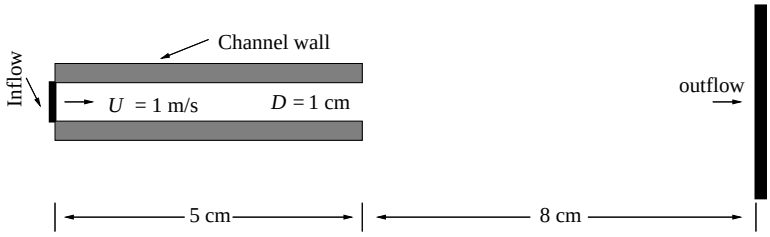

Figure 6. Domain specification for the simulation of the extrudate swell of a Second Order fluid.

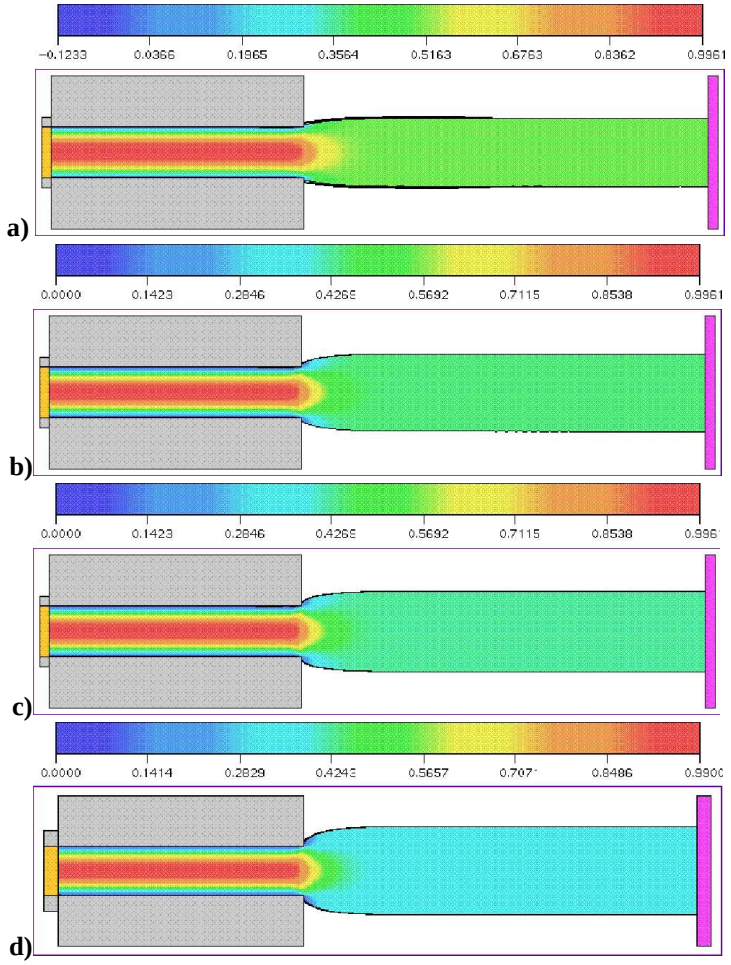

Figure 7. Numerical simulation of the extrudate swell for various Deborah numbers at $t = 0.9$ s. Fluid flow visualization and contours of the u-velocity. **a)** $De = 0.2, S_r = 1.42$, **b)** $De = 0.4, S_r = 1.55$, **c)** $De = 0.6, S_r = 1.64$, **d)** $De = 0.8, S_r = 1.85$.

5. Conclusions

This paper presented a finite difference technique for solving the governing equations for two-dimensional free surface flows of a second order fluid. The finite difference equations have been implemented into the Freeflow2D code (see Doricio (2003)) which was applied to simulate fully developed flow in a two-dimensional channel. The numerical results were compared to the analytic solution and the agreement was found to be good. Mesh refinement was used to demonstrate the convergence of the numerical method. The extrudate swell problem was simulated for various values of the Deborah number and the results showed that the numerical technique developed in this work can cope with high elastic fluids governed by the second order fluid constitutive equation.

6. References

Batchelor, G. K. 1967. "An Introduction to Fluid Dynamics". Cambridge Univ. Press, Cambridge.

Bird, R. B., Armstrong, R. C., and Hassager, O. 1987. "Dyanmics of Polymeric Liquids". John Willey & Sons, New York.

Brasseur, E., Fyrillas, M. M., Georgiou, G. C., and Crochet, M. J. 1998. "The Time-dependent Extrudate-swell Problem of an Oldroyd-B Fluid with Slip along the Wall". Journal of Reology, 42(3):549–566.

Carew, E. O. A., Townsend, P., and Webster, M. F. 1993. "A Taylor-Petrov-Galerkin Algorithm for Viscoelastic Flow". Journal of Non-Newtonian Fluid Mechanics, 50:253–287.

Cormenzana, J., Ledda, A., Laso, M., and Debbaut, B. 2001. "Calculation of Free Surface Flows using CONNFESSITT". Journal of Rheology, 45:237–258.

Crochet, M. J. and Keunings, R. 1982. "Finite Element Analysis of Die-swell of a Highly Elastic Fluid". Journal of Non-Newtonian Fluid Mechanics, 10:339–356.

Crochet, M. J. and Keunnings, R. 1980. "Die Swell of a Maxwell Fluid - Numerical Prediction". Journal of Non-Newtonian Fluid Mechanics, 7:199–212.

Doricio, J. L. 2003. "GENSMAC-SOF: Um Método Numérico para Simular Escoamentos Incompressíveis de Fluidos de Segunda Ordem". ICMC-USP - master thesis.

Ferreira, V. G., Tomé, M. F., Mangiavacchi, N., Castelo, A., Cuminato, J. A., Fortuna, A., and Mckee, S. 2002. "High Order Upwinding and the Hydraulic Jump". International Journal of Numerical Methods in Fluids, 39:549–583.

Gast, L. and Ellingson, W. 1999. "Die Swell Measurements of Second Order Fluids: Numerical Experiments". International Journal of Numerical Methods in Fluids, 29:1–18.

Griebel, M., Dornseifer, T., and Neunhoeffer, T. 1999. "Numerical Simulation in Fluid Dynamics: A Practical Introduction". SIAM.

Harlow, F. and Welch, J. E. 1965. "Numerical Calculation of Time-dependent Viscous Incompressible Flow of Fluid with a Free Surface". Phys. Fluids, 8:2182–2189.

Huang, X., Phan-Thien, N., and Tanner, R. I. 1996. "Viscoelastic Flow between Eccentric Rotating Cylinders: Unstructured Control Volume Method". Journal of Non-Newtonian Fluid Mechanics, 64:71–92.

Marchal, J. M. and Crochet, M. J. 1987. "A New Mixed Finite Element for Calculating Viscoelastic Flow". Journal of Non-Newtonian Fluid Mechanics, 26:77–114.

McKee, S., Tomé, M. F., Castelo, A., Cuminato, J. A., and Ferreira, V. G. 2003. "Recent Advances in the Marker and Cell Method". Archives of Computational Methods in Engineering, 11(2):107–142.

Mompean, G. and Deville, M. 1997. "Unsteady Finite Volume of Oldroyd-B Fluid through a Three-dimensional Planar Contraction". Journal of Non-Newtonian Fluid Mechanics, 72:253–279.

Phillips, T. N. and Williams, A. J. 1999. "Viscoelastic Flow through a Planar Contraction using a Semi-Lagrangian Finite Volume Method". Journal of Non-Newtonian Fluid Mechanics, 87:215–246.

Ryan, M. E. and Dutta, A. 1981. "A Finite Difference Simulation of Extrudate Swell". Pro. 2nd. World Congr. Chem. Eng., VI:277–281.

Sato, T. and Richardson, S. M. 1994. "Explicit Numerical Simulation of Time-dependent Viscoelastic Flows Problems by a Finite Element/Finite Volume Method". Journal of Non-Newtonian Mechanics, 51:249–275.

Shyy, W. 1997. "Computational Modeling for Fluid Flow and Interfacial Transport". Elsevier, Amsterdam.

Tanner, R. I. 1970. "A Theory of Die-swell". Journal of Polymer Science, 8:2067–2078.

Tomé, M. F., Duffy, B., and McKee, S. 1996. "A Numerical Method for Solving Unsteady Non-Newtonian Free Surface Flows". Journal of Non-Newtonian Fluid Mechanics, 62:9–34.

Tomé, M. F., Mangiavacchi, N., Cuminato, J. A., Castelo, A., and McKee, S. 2002. "A Finite Difference Technique for Simulating Unsteady Viscoelastic Free Surface Flows". Journal of Non-Newtonian Fluid Mechanics, 106:61–106.

Tomé, M. F. and McKee, S. 1994. "GENSMAC: A Computational Marker-and-cell Method for Free Surface Flows in General Domains". Journal of Computational Physics, 110:171–186.

Varonos, A. and Bergeles, G. 1998. "Development and Assessment of a Variable-order Non-oscillatory Scheme for Convection Term Discretization". International Journal of Numerical Methods in Fluids, 26:1–16.

Xue, S. C., Phan-Thien, N., and Tanner, R. I. 1998. "Three-dimensional Numerical Simulations of Viscoelastic Flows through Planar Contractions". Journal of Non-Newtonian Fluid Mechanics, 74:195–245.

Yoo, J. Y. and Na, Y. 1991. "A Numerical Study of the Planar Contraction Flow of a Viscoelastic Fluid using the SIMPLER Algorithm". Journal of Non-Newtonian Fluid Mechanics, 30:89–106.

7. Responsibility notice

The authors are the only responsible for the printed material included in this paper.